Raman scattering investigation of a $Ge/SiO_2/Si$ nanocrystal system under hydrostatic pressure

Lei Liu,[1] K. L. Teo,[2,*] Z. X. Shen,[1] J. S. Sun,[3] E. H. Ong,[3] A. V. Kolobov,[4] and Y. Maeda[5]
[1]*Physics Department, Blk. S12, Faculty of Science, National University of Singapore, 2 Science Drive 3, 117542 Singapore*
[2]*Department of Electrical and Computer Engineering, National University of Singapore, 4 Engineering Drive 3, 117576 Singapore*
[3]*Mechatronics & Micro System Group, Data Storage Institute, 117608 Singapore*
[4]*Center for Applied Near-Field Optics Research (CANFOR), National Institute of Advanced Industrial Science and Technology, Tsukuba Central 4, 1-1-1 Higashi, Tsukuba, Ibaraki 305-8562, Japan*
[5]*Department of Energy Science and Technology, Kyoto University, Sakyo-ku, Kyoto 606-8501, Japan*
(Received 22 July 2003; revised manuscript received 27 October 2003; published 23 March 2004)

We have studied the hydrostatic pressure dependence of Ge nanocrystals embedded in a SiO_2 matrix on a Si substrate by Raman scattering at room temperature. During the first cycle of increasing pressure, we observed a step change in the Ge Raman mode from 310.4 to 313.8 cm^{-1} at $\sim$23 kbar. The linear pressure coefficients α obtained before and after the step change at $\sim$23 kbar are 0.42 and 0.64 $cm^{-1}\,kbar^{-1}$, respectively. Upon decreasing pressure, the Ge mode follows a single slope of pressure coefficient $\alpha=0.64$ $cm^{-1}\,kbar^{-1}$. A finite-element analysis was carried out to investigate the elastic-field distribution in the $Ge/SiO_2/Si$ nanocrystal system, where the discontinuity of the specific geometric configuration with different elastic constants causes local areas of stress concentration around the interface. The step change of the Raman shifts with pressure at $\sim$23 kbar was attributed to complete delamination between the SiO_2 film and the Si substrate.

DOI: 10.1103/PhysRevB.69.125333 PACS number(s): 78.30.Am, 61.46.+w, 62.25.+g, 62.50.+p

INTRODUCTION

Generally in the nanocrystal-matrix systems, the distribution of the stress and strain field plays an important role in deciding the physical and thermodynamic properties of nanocrystals (NCs). It is well known that self-assembled NCs, such as the Ge/Si islands,[1–6] nucleate into ordered nanostructures via the Stranski-Krastanov growth mode as a result of strain accumulated due to the lattice mismatch. Strain in coherently embedded Ge/Si islands is also known to modify significantly the electronic properties of this nanostructure.[7] On Si(001), the NCs of epitaxial Ge were found effectively to repel one another strongly via the strain fields that are produced in the Si substrate.[8] It is also well understood that the common driving force for the self-organization of ordered arrays of uniform, coherent strained islands on crystal surfaces is the elastic interaction.[9,10] Thus, investigations on the elastic field in the nanocrystal-matrix systems would enhance our understanding of the strain mechanism of the NCs as well as the exploitation of their novel functions.

One of the most powerful methods to access information on strain in embedded nanostructures is Raman scattering spectroscopy.[11,12] With the application of pressure in Raman scattering,[11–15] strain in Ge layers is reduced due to the difference in compressibility between Si and Ge. We have previously reported a smaller pressure coefficient ($\alpha=d\omega/dp=0.34$ $cm^{-1}\,kbar^{-1}$) obtained for the Ge mode in Ge/Si islands[11] and Ge/Si dot superlattices[12] on Si substrates as compared with the corresponding bulk value ($\alpha=0.39$ $cm^{-1}\,kbar^{-1}$). This is attributed to the fact that Ge islands are strongly constrained by the surrounding Si lattice, leading to a smaller deformation as compared to the bulk Ge, when subject to the same pressure. Recently, we have also shown that for Ge NCs embedded in a glass matrix, the pressure coefficient ($\alpha=0.77$ $cm^{-1}\,kbar^{-1}$) obtained for the Ge mode is almost twice as large as its corresponding bulk value.[16] This can be explained using a simple elastic model, which describes the effective pressure transmitted from the matrix to the nanocrystals. However, the interface strain/stress effects under applied hydrostatic pressure have not been fully understood in a more complicated nanocrystal system, such as Ge or Si NCs embedded in SiO_2 on a Si substrate. For example, in the high-pressure photoluminescence (PL) measurement of Si NCs in SiO_2 layers on the Si substrate by Cheong *et al.*,[17] the observed pressure coefficients of the PL peak energy on the two Si NCs samples *A* and *B* gave different values (-0.4 and -0.6 meV/kbar) separately, which were not in good quantitative agreement with an estimate based on the quantum confinement model. Both of these two samples were formed by ion implantation of Si^+ ions into thermally oxidized Si wafers followed by thermal annealing, but with a different thickness of SiO_2 layers. Moreover, in the first pressure cycle on sample *B* (thicker one) a considerable hysteresis was observed but not in the second cycle. Cheong *et al.* suggested that the initial hysteresis was due to an irreversible pressure-induced relief of built-in strains in the nanocrystals, but no explanation was given for why this particular sample has built-in strains. Therefore, it is necessary and timely to carry out high-pressure researches further on the multicomponent nanocrystal system to elucidate the strain/stress effect on the NCs in the nanostructures. Moreover, since desired functional characteristics of a semiconductor heterostructure depend crucially on their structure and geometry, which are generally influenced by the local elastic field distribution during its fabrication or application, further investigations on multicomponent nanostructures, such as the $Ge/SiO_2/Si$ nanocrystal system, may give some insight into exploring the formation or application of semiconductor nanostructures.

In this paper, we report on the high-pressure Raman scattering investigations on Ge NCs embedded in a SiO_2 matrix

on Si substrate. In this nanocrystal system in which the Ge NCs and the Si substrate have a different Raman frequency (Ge mode $\sim 300\ \mathrm{cm}^{-1}$ and Si mode $\sim 521\ \mathrm{cm}^{-1}$), it would be much easier to make clearer the different strain effects on the NCs and the substrate than on the $Si/SiO_2/Si$ nanocrystal system. It is noted that the Si acoustic peak at $\sim 300\ \mathrm{cm}^{-1}$ can be eliminated by specific polarization configuration.[12] Moreover, our experiments[11,12,16] suggested that the Raman shifts with pressure ($\alpha = d\omega/dp$) are independent of the size of the NCs, which is consistent with the common understanding[18] based on the high-pressure Raman experiments on CdS and CdSe that the potential energy as a function of unit cell volume is identical in both the harmonic and the first anharmonic term in tetrahedrally bonded bulk and nanocrystal systems. This simplifies the study of the mechanism of the elastic field evolution with the surrounding hydrostatic pressure, since we can neglect the size effect of the NCs.

EXPERIMENT

The samples for investigation were prepared by codeposition of Ge and SiO_2 by radio-frequency (rf) magnetron sputtering onto a Si(001) substrate with about 3–5-nm-thick native oxide. The sample thickness is $\sim 1\ \mu$m and Ge concentration is ~ 60 mol. %. After deposition, the sample was annealed for 1 h at 800 °C in an argon atmosphere, which produced the NCs. More details on the sample preparation can be found elsewhere.[19]

Figure 1(a) shows the transmission electron microscopic (TEM) image of the annealed Ge NCs.[20] Interestingly, the NCs are preferentially formed in the area away from the sample surface, and at the interface with the silicon substrate the density of the NCs is somewhat higher. High-resolution (HR) TEM images [Figs. 1(b) and 1(c)] reveal other features of the formed NCs.[20] The NCs formed in bulk of the sample have clearly pronounced facets and are single crystals, in very few cases with twinning defects. The NCs formed in the direct vicinity of the Si substrate, on the other hand, are spherical and the interface under these NCs is no longer flat. The size of the NCs, ~ 20 nm, is almost the same in both cases.

The Raman spectra were recorded in a backscattering geometry at room temperature using a 514.5-nm line from an argon-ion laser. The scattered spectra were analyzed with a Jobin-Yvon T64000 triple-grating micro-Raman system. The pressure-dependent measurements were carried out using a standard diamond anvil cell technique with a 4:1 mixture of methanol and ethanol as the pressure-transmitting medium. The applied pressures were monitored by the shift of the ruby R1 line.

RESULTS AND DISCUSSION

Figure 2(a) shows the Raman spectra for the $Ge/SiO_2/Si$ sample at ambient pressure. The Ge mode occurs at $\sim 300\ \mathrm{cm}^{-1}$ with a full width at half maximum (FWHM) of about $5\ \mathrm{cm}^{-1}$ while the Si mode from the substrate is at $\sim 521\ \mathrm{cm}^{-1}$ with a FWHM of about $4\ \mathrm{cm}^{-1}$. The appearance of a strong and sharp peak of the Ge mode indicates the formation of the crystalline phase. We have used the polarization configuration $z(x,y)\bar{z}$ (z along the [001] direction, x along the [100] direction, and y along the [010] direction of the Si substrate) to minimize the Si acoustic phonon peak at $\sim 303\ \mathrm{cm}^{-1}$.[12] We note that the Ge mode shifts to lower frequency as the laser intensity increases. To prevent any laser-induced heating, the laser power on the sample is kept to a minimum with a power density of $\sim 5\times 10^4\ \mathrm{W/cm}^2$.

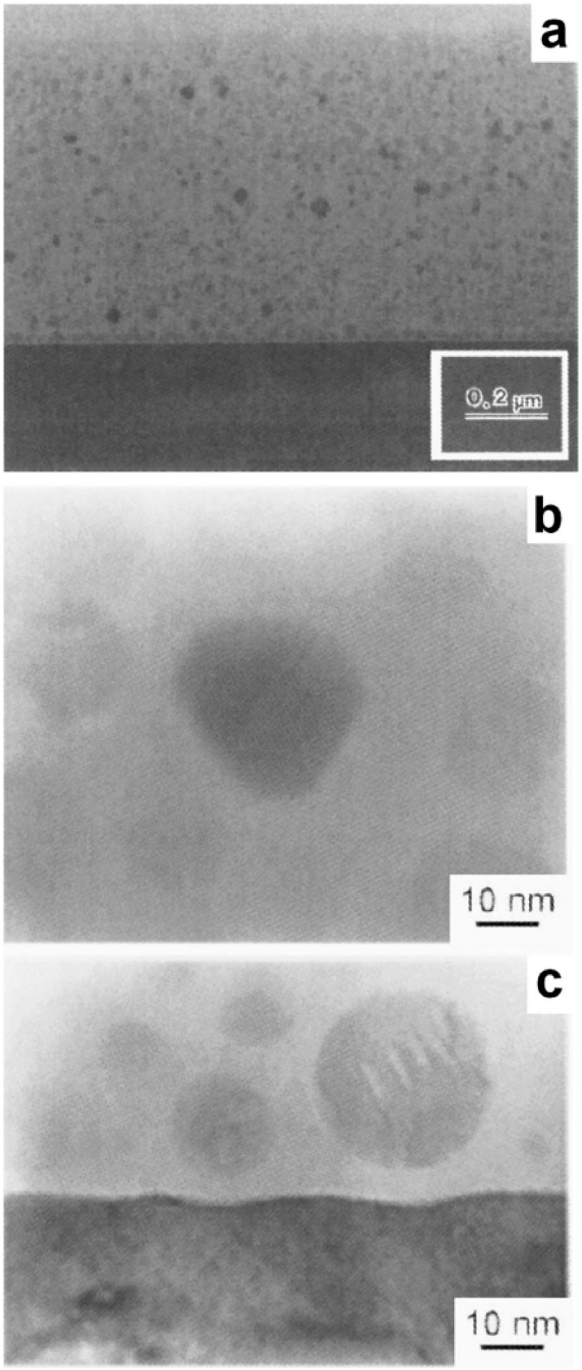

FIG. 1. (a) TEM image of $Ge/SiO_2/Si$ NC samples; (b) HR-TEM image of $Ge/SiO_2/Si$ NC samples with Ge NCs formed in the bulk of the sample; and (c) in the vicinity of the Si(001) interface.

The Raman shifts of the Ge mode and the Si mode with

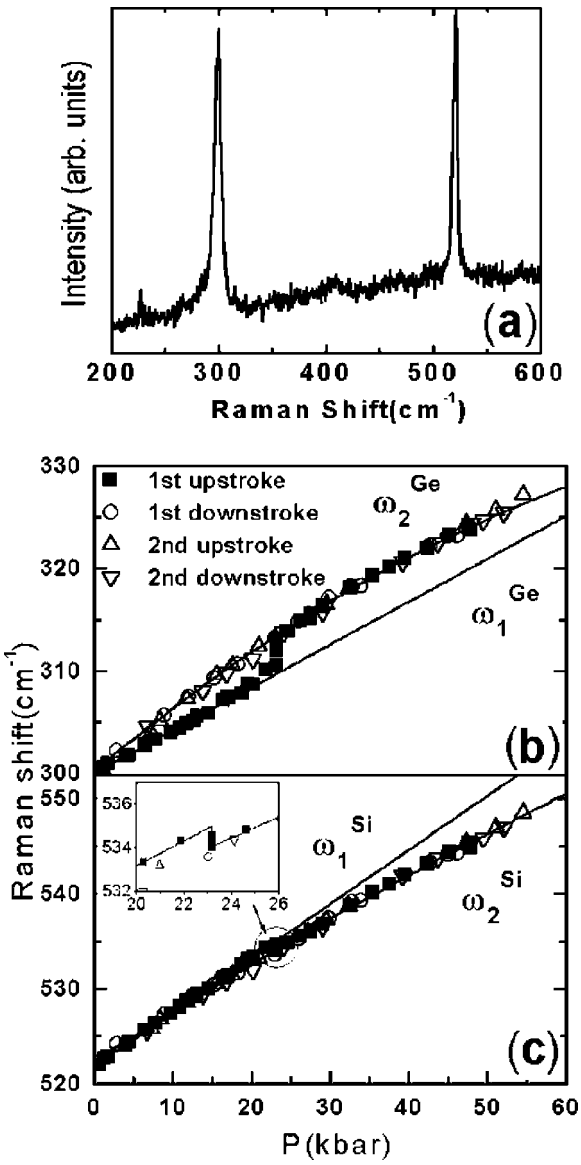

FIG. 2. Raman spectra for $Ge/SiO_2/Si$ NC samples at ambient pressure (a); pressure dependence of Raman shift of the Ge mode (b); and the Si mode (c). The inset shows the enlarged portion of the Si mode near transition $P \sim 23$ kbar.

pressure P for two pressure cycles were shown in Figs. 2(b) and 2(c), where both the Ge and the Si peaks were fitted to the Lorentzian profile. During the first upstroke of the pressure cycle, the Ge mode shifts linearly with P and then shows a step that jumps up from 310.4 to 313.8 cm^{-1} at $P \sim 23$ kbar, and subsequently shifts up with P at a higher pressure coefficient (α). On the other hand, at $P \sim 23$ kbar, the Si mode shifts down by ~ 0.9 cm^{-1}, and thereafter the Si mode shifts up at a lower pressure coefficient (α). Our results show that at $P \sim 23$ kbar in the first upstroke of pressure, there exists an irreversible transition in the strain effect of the $Ge/SiO_2/Si$ nanocrystal system. In the last part of the first upstroke (i.e., beyond 23 kbar) and the first downstroke, α remained unchanged. The second pressure cycle shows that both the Ge and Si modes keep the reversible Raman shift with pressure with the same α as the first downstroke of the

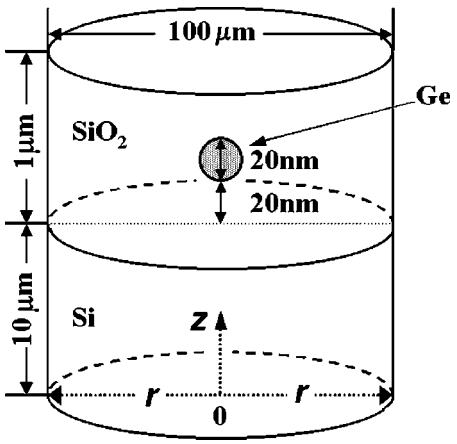

FIG. 3. Schematic structure of the $Ge/SiO_2/Si$ axis symmetrical nanocrystal system modeled.

pressure cycle. It is noteworthy that although the present high pressure experiment is performed on Ge NCs of size ~ 20 nm, we have also observed similar behavior in Ge NCs of size 4–12 nm with the same SiO_2 layer thickness, indicating the observed phenomenon is independent of NC size.

As shown in Figs. 2(b) and 2(c), the solid curves correspond to the least-squares fits to the experimental data, where the Raman modes before (ω_1) and after (ω_2) the transition at $P \sim 23$ kbar were fitted separately,

$$\omega_1^{\mathrm{Ge}}(P) = (300.0 \pm 0.1) + (0.42 \pm 0.01)P, \tag{1}$$

$$\omega_2^{\mathrm{Ge}}(P) = (300.2 \pm 0.2) + (0.64 \pm 0.02)P - (0.003 \pm 0.001)P^2, \tag{2}$$

$$\omega_1^{\mathrm{Si}}(P) = (521.7 \pm 0.1) + (0.57 \pm 0.01)P, \tag{3}$$

$$\omega_2^{\mathrm{Si}}(P) = (522.3 \pm 0.2) + (0.53 \pm 0.01)P - (0.001 \pm 0.0002)P^2. \tag{4}$$

According to these fitting results, we found that after the irreversible transition at 23 kbar, α of the Ge mode changes from 0.42 to 0.64 cm^{-1} kbar^{-1} and α of the Si mode changes from 0.57 to 0.53 cm^{-1} kbar^{-1}. We note that the elastic field distribution would not be uniformly homogeneous in the $Ge/SiO_2/Si$ nanocrystal system, especially near the interface between the SiO_2 matrix and the Si substrate. Thus, it is necessary to investigate the elastic-field distribution in the $Ge/SiO_2/Si$ nanocrystal system to enhance our understanding of the pressure dependence of the Raman shifts of the Ge and Si modes.

Using a finite-element package (ABAQUS/Standard), an axisymmetric model structure as shown in Fig. 3, where the Ge NC sphere is embedded along the rotation z axis, and the Si substrate and SiO_2 matrix cylindrical layers are separated by a sharp interface, was chosen to study the elastic-field distribution in the nanocrystal system under a hydrostatic pressure of 10 kbar. For simplicity, the Ge NCs, SiO_2 matrix, and Si substrate were considered as isotropic elastic continua, with elastic constants of Ge ($E_1 = 1316.6$ kbar, σ_1

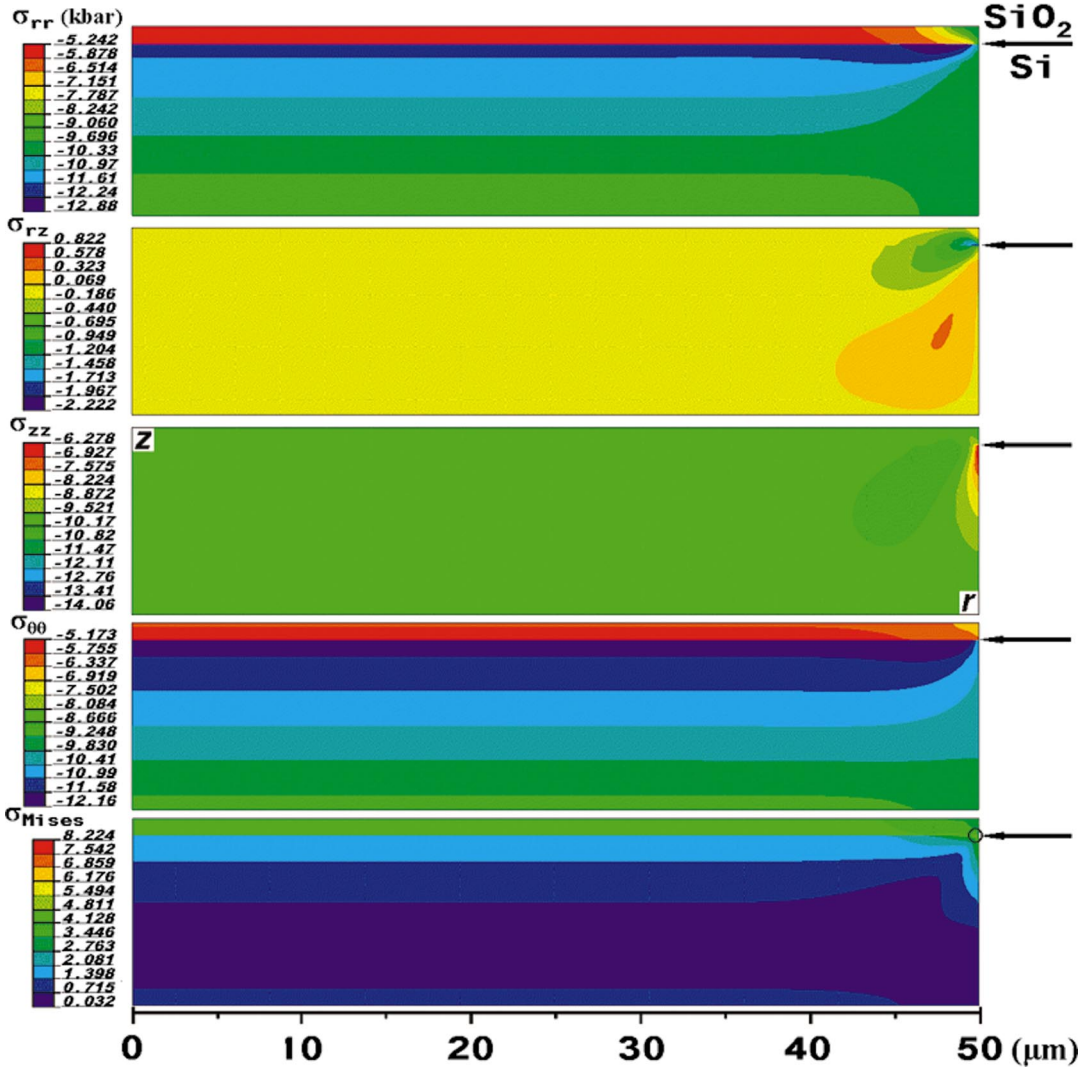

FIG. 4. (Color) Global $r-z$ plane stress distributions of σ_{rr}, σ_{rz}, σ_{zz}, $\sigma_{\theta\theta}$, and σ_{Mises} for the disk-shaped $\mathrm{Ge/SiO_2/Si}$ nanocrystal system, with the arrows pointed at the $\mathrm{SiO_2/Si}$ interface.

$=0.207\,48$, $K_1=750.17$ kbar),[21] of $\mathrm{SiO_2}$ ($E_2=730$ kbar, $\sigma_2=0.162$, $K_2=361$ kbar),[22] and of Si ($E_3=1629.1$ kbar, $\sigma_3=0.222\,62$, $K_3=978.87$ kbar) (Ref. 21) separately. Here $(E_i,\sigma_i,K_i)_{i=1,2,3}$ are Young's modulus, Poisson's ratio, and the bulk modulus, respectively.

Figure 4 shows the $r-z$ plane stress distributions of σ_{rr}, σ_{rz}, σ_{zz}, $\sigma_{\theta\theta}$, and σ_{Mises} for the disk-shaped $\mathrm{Ge/SiO_2/Si}$ nanocrystal system, where the negative values indicate the compressive stress. All five stress tensors are distributed rather nonhomogeneously around the surface of the nanocrystal system and near the $\mathrm{SiO_2/Si}$ interface. But in the central part of the nanocrystal system away from the periphery, the five tensors are distributed uniformly in the layers parallel to the $\mathrm{SiO_2/Si}$ interface. At the $\mathrm{SiO_2/Si}$ interface, there is a significant discontinuity for σ_{rr} and $\sigma_{\theta\theta}$. The values of σ_{rr} and $\sigma_{\theta\theta}$, which are almost identical in the central part, jump from about -5.70 kbar at the $\mathrm{SiO_2}$ matrix to about -11.77 kbar at the Si substrate. This can be ascribed to the fact that $\mathrm{SiO_2}$ ($K_2=361$ kbar) is much easier to compress than Si ($K_3=978.87$ kbar), but both of them have to shrink together at the interface under pressure. As a result, the $\mathrm{SiO_2}$ matrix experiences more tensile stress near the $\mathrm{SiO_2/Si}$ interface than anywhere else. On the other hand, the Si substrate has to undergo a more compressive stress. Accordingly, the absolute values of σ_{rr} and $\sigma_{\theta\theta}$ for the $\mathrm{SiO_2}$ matrix become smaller from the top surface to the $\mathrm{SiO_2/Si}$ interface, while σ_{rr} and $\sigma_{\theta\theta}$ of the Si substrate become bigger from the bottom surface to the $\mathrm{SiO_2/Si}$ interface. Consequently, before the transition at 23 kbar, the α of Ge ($\sim 0.42\ \mathrm{cm^{-1}\,kbar^{-1}}$) and Si modes ($\sim 0.57\ \mathrm{cm^{-1}\,kbar^{-1}}$) can be due to the discontinuous distribution of σ_{rr} and $\sigma_{\theta\theta}$ in the nanocrystal system introduced by the $\mathrm{SiO_2/Si}$ interface. As a result of the concentration of the discontinuous stresses, the interface strain would accumulate accordingly, which may induce the debonding of the $\mathrm{SiO_2/Si}$ interface, i.e., the delamination between the $\mathrm{SiO_2}$ matrix and the Si substrate layers. The delamination behavior of the $\mathrm{SiO_2/Si}$ interface could be further understood by the distribution of (Von) Mises stress[23] σ_{Mises} (Fig. 4). The local distribution of σ_{Mises} at the peripheral $\mathrm{SiO_2/Si}$ interface edge (the enlarged circle

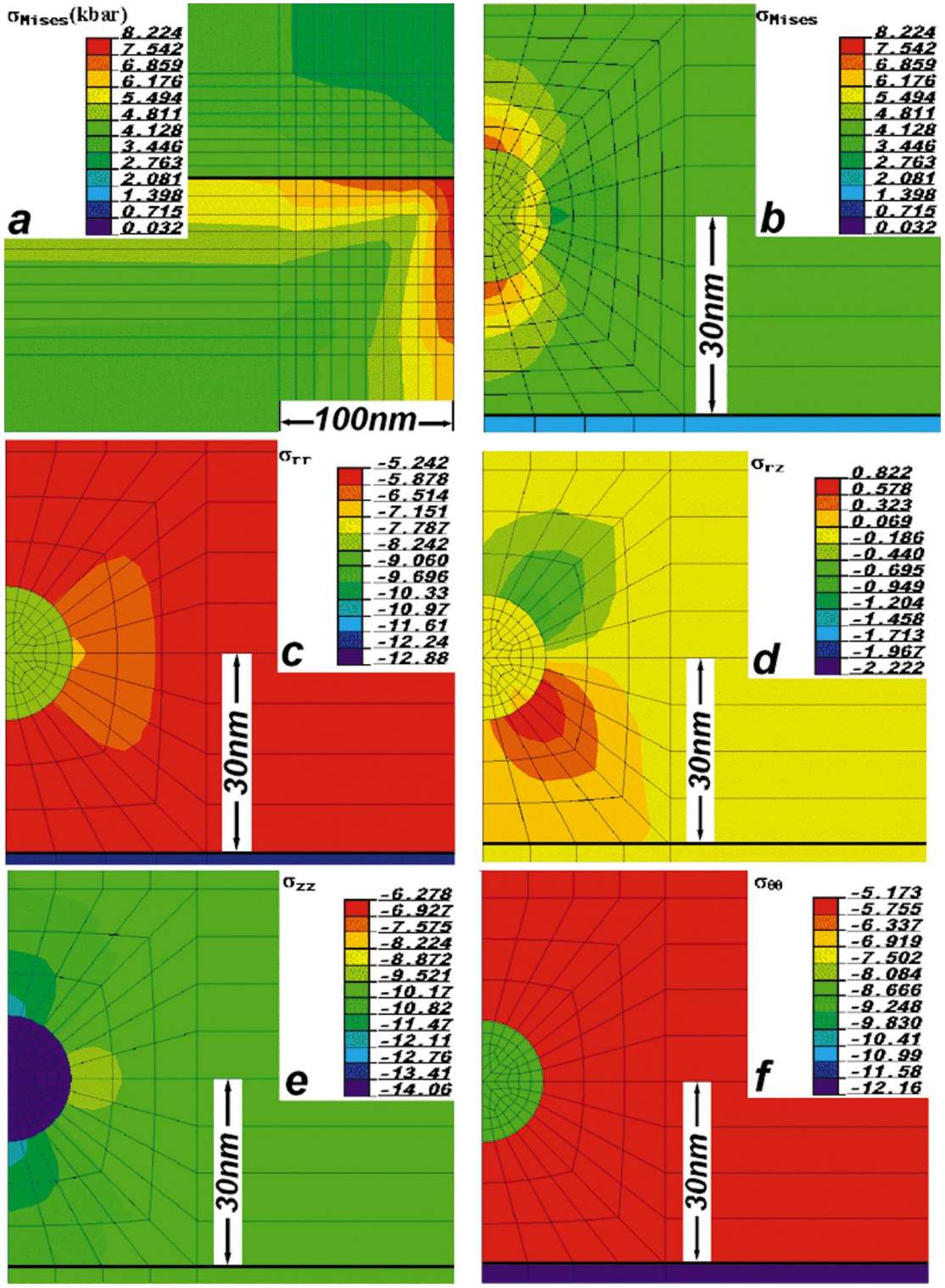

FIG. 5. (Color) Local $r-z$ plane (Von) Mises stress distribution (a) of σ_{Mises} near the peripheral SiO_2/Si interface edge (the enlarged circle part in Fig. 4), and the local $r-z$ plane stress distribution of σ_{Mises} (b), σ_{rr} (c), σ_{rz} (d), σ_{zz} (e), and $\sigma_{\theta\theta}$ (f) around a Ge NC, where the thin sold lines indicate the meshes used in the calculation while the thicker line indicates the SiO_2/Si interface.

part in Fig. 4) was magnified as shown in Fig. 5(a), together with the local stress distribution of σ_{Mises}, σ_{rr}, σ_{rz}, σ_{zz}, and $\sigma_{\theta\theta}$ around Ge NCs (embedded along the rotation z axis, as shown in Fig. 3). The distribution of σ_{Mises} concentrates strongly at the outer SiO_2/Si interface edge ($r=r_{\max}=50\ \mu$m), which indicates further that the delamination could start from the edge where the largest strain energy is accumulated and gradually move inwards. Due to this delamination behavior, we are able to explain our experimental observation for the discontinuity at $P\sim 23$ kbar.

As the optical penetration depth of a 514.5-nm laser in Si(001) is about 1.0 μm,[24] the Si substrate layer of 1.0-μm thickness below the SiO_2/Si interface contributes mainly to the observed Si Raman signal. In this layer, due to the bounding at the SiO_2/Si interface, the absolute value of ε_{zz} is smaller than those of ε_{rr} and $\varepsilon_{\theta\theta}$ in the central part of the Si substrate. In the Si substrate close to the SiO_2/Si interface, the calculated strains ε_{rr} and $\varepsilon_{\theta\theta}$ are $\sim -4.24\times10^{-3}$ and ε_{zz} is $\sim -2.92\times10^{-3}$. In the Si substrate layer, 1.0 μm below the SiO_2/Si interface, the calculated strains ε_{rr} and $\varepsilon_{\theta\theta}$ have the values of -4.15×10^{-3} and ε_{zz} has the value of -2.98×10^{-3}. The calculated strain ε_{rz} is almost zero in the central part of the Si substrate. It is known that as strain is applied along the major crystal axes of the cubic crystal, the triply degenerate optical mode (here for the $\Gamma_{25'}$ Si optical phonon) near zero wave vector is split into a singlet and a doublet.[13,25,26] In backscattering geometry along the [001] direction, only the singlet is observed, and the Raman frequency of the Si mode, in the absence of interfacial disorder, is

$$\omega = \omega_0 + (1/2\omega_0)[p\varepsilon_{zz} + q(\varepsilon_{rr} + \varepsilon_{\theta\theta})], \tag{5}$$

where $\omega_0 (=0.9849\times10^{14}\ s^{-1})$ is the frequency of the c-Si zone-center longitudinal-optical phonon, and p $(=-1.345\times10^{28}\ s^{-2})$ and q $(=-1.946\times10^{28}\ s^{-2})$ are the Si deformation potentials.[13,25,26]

Consequently, before delamination the pressure coefficient α of the Si mode has the value of 0.55 $cm^{-1}\,kbar^{-1}$ for the Si substrate near the SiO_2/Si interface and of 0.54 $cm^{-1}\,kbar^{-1}$ for the Si substrate 1.0 μm below the SiO_2/Si interface. After delamination, the pressure coefficient α of the Si mode is $\sim$0.48 $cm^{-1}\,kbar^{-1}$ as of the bulk Si, which has $\varepsilon_{rr}=\varepsilon_{\theta\theta}=\varepsilon_{zz}=3.405\times10^{-3}$ under a hydrostatic pressure of 10 kbar. Thus the calculated downshift of the Si mode at the delamination of $\sim$23 kbar is about 1.4 cm^{-1}. This result agrees reasonably well with our experimentally observed downshifts of $\sim$0.9 cm^{-1} (α changes from 0.57 to 0.53 $cm^{-1}\,kbar^{-1}$) within the experimental error bars. The behavior of the optical phonon from the Ge NCs with pressure could be understood similarly. The Ge NCs are formed in the SiO_2 matrix without preferential orientation. The broadening of the Raman mode can be due to the average strain effect together with phonon confinement as well as size distribution.

From the local stress distributions around Ge NCs (Fig. 5), we can further understand the characteristics of the Ge/SiO_2/Si nanocrystal system. Due to the smaller compressibility of Ge ($K_1=750.17$ kbar) NCs than the SiO_2 ($K_2=361$ kbar) matrix, Ge NCs undergo larger stresses of σ_{rr}, σ_{zz}, and $\sigma_{\theta\theta}$ than the surrounding SiO_2 matrix. Moreover, the discontinuous and nonuniform stress distribution of σ_{rr}, σ_{rz}, σ_{zz}, and $\sigma_{\theta\theta}$ can be observed around the Ge/SiO_2 interface. In the SiO_2 matrix, the existence of Ge NCs effectively modified the surrounding elastic field of a nonuniform stress distribution with a scale comparable to the size of the NCs. Similarly, Ge NCs can also introduce nonuniform local stress during cooling or heating in the high-temperature growth of the Ge/SiO_2/Si nanocrystal system due to different thermal-expansion coefficients. The roughness of the Si/SiO_2 interface under the NCs with the local geometry corresponding to the shape of NCs, as shown in Fig. 1(c), could be due to the nonhomogeneous local stress distribution induced by the embedded Ge NCs during fabrication.

From the above discussions, our high-pressure Raman results on the Ge/SiO_2/Si nanocrystal system can be explained by its nonhomogeneous distribution of the elastic field under pressure due to the specific geometric configuration of different parts with different elastic constants. The transition at 23 kbar can be ascribed to the delamination of the SiO_2/Si interface as a result of the accumulated strain energy. Accordingly, the Raman shift of the Ge mode and the Si-Si mode with pressure can be easily understood. Before the transition, $\alpha=0.57\ cm^{-1}\,kbar^{-1}$ of the Si mode in the first upstroke of the pressure cycle can be ascribed to the more compressive σ_{rr} and $\sigma_{\theta\theta}$ introduced by the SiO_2/Si interface. After the delamination, since the interface stress is released, the Si mode shifts down by 0.9 cm^{-1} and $\alpha=0.53\ cm^{-1}\,kbar^{-1}$ recovers to almost the bulk value.[14] On the other hand, before the transition, $\alpha=0.42\ cm^{-1}\,kbar^{-1}$ of the Ge mode is due to more local tensile σ_{rr} and $\sigma_{\theta\theta}$ in the SiO_2 matrix introduced by the SiO_2/Si interface. After the delamination, as the interface stress is released, without the shielding from the Si substrate, the Ge mode shifts to a higher wave number by 3.4 cm^{-1} and α changes to 0.64 $cm^{-1}\,kbar^{-1}$ thereafter. However, due to the fact that the Ge NCs are distributed in a rather thin SiO_2 matrix layer of ~1 μm, the stress concentration of σ_{rr}, σ_{zz}, and $\sigma_{\theta\theta}$ on the Ge NCs is relatively smaller than that on the Ge NCs embedded deep in the SiO_2 matrix on a quartz substrate, thus α $(=0.64\ cm^{-1}\,kbar^{-1})$ in the Ge/SiO_2/Si nanocrystal system is still smaller than that of the Ge/SiO_2/quartz nanocrystal system ($\alpha=0.77\ cm^{-1}\,kbar^{-1}$).[16] Since the delamination is irreversible, the second pressure cycle (second upstroke and second downstroke) shows that both the Ge and Si modes keep the same α as the first downstroke of the pressure cycle.

We also calculated the dependence of σ_{rr} and $\sigma_{\theta\theta}$ on the thickness of the SiO_2 matrix layer, where the axisymmetric model structure as shown in Fig. 3 was still used but with the thickness of the SiO_2 layer varied from 0.2 μm to 3.0 μm. The calculated σ_{rr} and $\sigma_{\theta\theta}$ near the SiO_2/Si interface around the central rotation axis, i.e., $r\rightarrow0$, as a function of the thickness of the SiO_2 matrix layer are shown in Fig. 6. We found that as the thickness of the SiO_2 matrix layer increases, the stress concentration of σ_{rr} and $\sigma_{\theta\theta}$ in the Si substrate gets stronger accordingly and the difference between the two sides of the SiO_2/Si interface also becomes bigger, and as a result more strain energy would accumulate around the SiO_2/Si interface. Thus, in the nanocrystal system, under the same pressure, the delamination will occur more easily for a thicker SiO_2 matrix layer as compared with the one in the nanocrystal system with a thinner SiO_2 matrix.

In addition, our model can explain the seemingly confusing results for the high-pressure PL measurement on the Si/SiO_2/Si nanosystem in the literature.[17] In that experiment, a step change of PL peak shift with pressure around 12 kbar

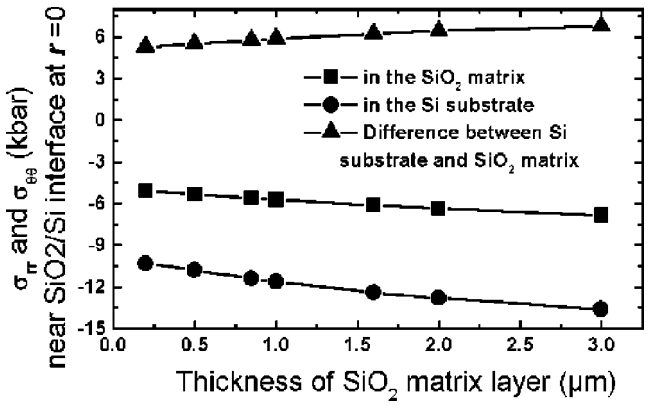

FIG. 6. Calculated σ_{rr} and $\sigma_{\theta\theta}$ near the SiO_2/Si interface at $r \rightarrow 0$ as a function of the thickness of the SiO_2 matrix layer.

was observed in the first pressure cycle only in sample *B* (with a SiO_2 layer thickness of 1.6 μm), but not in sample *A* (with a SiO_2 layer thickness of 0.83 μm) in the whole range below 46 kbar. Moreover, the observed pressure coefficient of the PL peak energy of Si NCs samples *A* and *B* has different values of -0.4 and -0.6 meV/kbar, respectively. Under the same pressure, the interface delamination is apt to take place with the thicker SiO_2 matrix layer than with the thinner one. Hence, on the Si/SiO_2/Si nanocrystal system, the considerable hysteresis (delamination) around 12 kbar was observed in the first pressure cycle only in sample *B*, but not in sample *A*. This is also consistent with our observation of the delamination of the SiO_2/Si interface at 23 kbar on a Ge/SiO_2/Si nanocrystal system, with a SiO_2 layer thickness of 1.0 μm. The larger pressure coefficients (-0.6 meV/kbar) of the PL peak energy observed in sample *B* in the second pressure cycle than that (-0.4 meV/kbar) of sample *A* can be ascribed to the pressure coefficient after the SiO_2/Si interface delamination in sample *B*, since the Si NCs experience more compressive stress without the shielding of the Si substrate.

CONCLUSION

In conclusion, we have investigated the Ge/SiO_2/Si nanocrystal system by Raman scattering under hydrostatic pressure. We found that the delamination between a SiO_2 film and a Si substrate occurs at $\sim$23 kbar due to the large difference between the compressibility of the SiO_2 matrix and the Si substrate. The observed effect can be understood by the nonhomogeneous distribution of the elastic field in the Ge/SiO_2/Si nanocrystal system. Moreover, the previous unexplained high-pressure PL results on the Si/SiO_2/Si nanocrystal system can be explained by the nonuniform distribution of the elastic field. Although our investigation focuses on the Ge/SiO_2/Si nanocrystal system, our results could provide a general understanding of the elastic properties of different multicomponent nanocrystal systems.

*Electronic address: eleteokl@nus.edu.sg

[1] G. Wedler, J. Walz, T. Hesjedal, E. Chilla, and R. Koch, Phys. Rev. Lett. **80**, 2382 (1998).
[2] F. M. Ross, J. Tersoff, and R. M. Tromp, Phys. Rev. Lett. **80**, 984 (1998).
[3] I. Goldfarb, P. T. Hayden, J. H. G. Owen, and G. A. D. Briggs, Phys. Rev. Lett. **78**, 3959 (1997).
[4] A. J. Steinfort, P. M. L. O. Scholte, A. Ettema, F. Tuinstra, M. Nielsen, E. Landemark, D.-M. Smilgies, R. Feidenhans'l, G. Falkenberg, L. Seehofer, and R. L. Johnson, Phys. Rev. Lett. **77**, 2009 (1996).
[5] C. P. Liu, J. M. Gibson, D. G. Cahill, T. I. Kamins, D. P. Basile, and R. S. Williams, Phys. Rev. Lett. **84**, 1958 (2000).
[6] S. A. Chaparro, J. Drucker, Y. Zhang, D. Chandrasekhar, M. R. McCartney, and D. J. Smith, Phys. Rev. Lett. **83**, 1199 (1999).
[7] O. G. Schmidt, K. Eberl, and Y. Rau, Phys. Rev. B **62**, 16 715 (2000).
[8] R. S. Williams, G. Medeiros-Ribeiro, T. I. Kamins, and D. A. A. Ohlbergy, Annu. Rev. Phys. Chem. **51**, 527 (2000).
[9] Z. I. Alferov, Rev. Mod. Phys. **73**, 767 (2001).
[10] V. A. Shchukin and D. Bimberg, Rev. Mod. Phys. **71**, 1125 (1999).
[11] K. L. Teo, L. Qin, Z. X. Shen, and O. G. Shmidt, Appl. Phys. Lett. **80**, 2919 (2002).
[12] L. Qin, K. L. Teo, Z. X. Shen, C. S. Peng, and J. M. Zhou, Phys. Rev. B **64**, 075312 (2001).
[13] Z. F. Sui, I. P. Herman, and J. Bevk, Appl. Phys. Lett. **58**, 2351 (1991).
[14] Z. F. Sui, H. H. Burke, and I. P. Herman, Phys. Rev. B **48**, 2162 (1993).
[15] M. Seon, M. Holtz, Ta-Ryeong Park, O. Brafman, and J. C. Bean, Phys. Rev. B **58**, 4779 (1998).
[16] L. Liu, Z. X. Shen, K. L. Teo, A. V. Kolobov, and Y. Maeda, J. Appl. Phys. **93**, 9392 (2003).
[17] H. M. Cheong, W. Paul, S. P. Withrow, J. G. Zhu, J. D. Budai, C. W. White, and D. M. Hembree, Jr., Appl. Phys. Lett. **68**, 87 (1996).
[18] S. H. Tolbert and A. P. Alivisatos, Annu. Rev. Phys. Chem. **46**, 595 (1995).
[19] Y. Maeda, Phys. Rev. B **51**, 1658 (1995).
[20] A. V. Kolobov, S. Q. Wei, W. S. Yan, H. Oyanagi, Y. Maeda, and K. Tanaka, Phys. Rev. B **67**, 195314 (2003).
[21] H. Ledbetter and S. Kim, in *Handbook of Elastic Properties of Solids*, edited by M. Levy, H. E. Bass, R. R. Stern, L. Furr, and V. Keppens (Academic Press, San Diego, 2001), Vol. II, pp. 99 and 100.
[22] L. Duffrene and J. Kieffer, in *Properties, Processing and Applications of Glass and Rare Earth-Doped Glasses for Optical Fibres*, edited by D. Hewak (IEE: INSPEC, London, 1998), p. 29.
[23] A. Saxena, in *Nonlinear Fracture Mechanics for Engineers*, edited by A. Saxena (CRC Press, Boca Raton, 1998), Chap. 2, p. 27.
[24] G. E. Jellison, Jr., Opt. Mater. (Amsterdam, Neth.) **1**, 41 (1992).
[25] F. Cerdeira, C. J. Buchenauer, F. H. Pollak, and M. Cardona, Phys. Rev. B **5**, 580 (1972).
[26] D. J. Lockwood and J.-M. Baribeau, Phys. Rev. B **45**, 8565 (1992).